Fully Differential Cross Sections for Photo-Double-Ionization of D_2

Th. Weber,[1,4,6] A. Czasch,[1] O. Jagutzki,[1] A. Müller,[1] V. Mergel,[1] A. Kheifets,[2] J. Feagin,[3] E. Rotenberg,[4] G. Meigs,[4]
M. H. Prior,[4] S. Daveau,[4] A. L. Landers,[5] C. L. Cocke,[6] T. Osipov,[6] H. Schmidt-Böcking,[1] and R. Dörner[1,*]

[1]*Institut für Kernphysik, Universität Frankfurt, D 60486 Frankfurt, Germany*
[2]*Research School of Physical Sciences and Engineering, Australian National University, Canberra ACT 0200, Australia*
[3]*Department of Physics, California State University–Fullerton, Fullerton, California 92834, USA*
[4]*Lawrence Berkeley National Laboratory, Berkeley, California 94720, USA*
[5]*Department of Physics, Western Michigan University, Kalamazoo, Michigan 49008, USA*
[6]*Department of Physics, Kansas State University, Manhattan, Kansas 66506 USA*

We report the first kinematically complete study of the four-body fragmentation of the D_2 molecule following absorption of a single photon. For equal energy sharing of the two electrons and a photon energy of 75.5 eV, we observed the relaxation of one of the selection rules valid for He photo-double-ionization and a strong dependence of the electron angular distribution on the orientation of the molecular axis. This effect is reproduced by a model in which a pair of photoionization amplitudes is introduced for the light polarization parallel and perpendicular to the molecular axis.

The simultaneous ejection of two electrons by the absorption of a single photon (photo-double-ionization or PDI) is a paradigm in the study of the dynamics of electron-electron correlation. However, only the simplest process of this kind, i.e., PDI of helium, is substantially well understood (see [1]). A more intricate PDI process is the photofragmentation of the H_2 (or D_2) molecule. Here the rapid departure of the two photoelectrons is followed by the Coulomb explosion of the two bare nuclei, and their relative momentum defines the molecular alignment, a reference axis essential to fully describe the process. As in He, one expects important effects from electron-electron repulsion, and selection rules, but also from additional electron-nuclei interactions, and the final state molecular symmetry. How do these combine to yield the four-body final state? To help elucidate these issues, we report here the first kinematically complete study of PDI from D_2; we point out the similarities and differences with PDI in He.

Pioneering experiments on PDI of H_2 measured the ion fragments and yielded the total cross section and the ion angular distribution ([2,3]). More recently, two-electron coincidence ($\gamma, 2e$) experiments (no ion detection) ([4–7]) and one-electron–two-ion coincidence measurements [8] became feasible. The ($\gamma, 2e$) results revealed surprising similarity of the electron angular distributions for He and D_2. For He, at energies up to 100 eV above threshold, these angular distributions (fully differential cross sections—FDCS) are governed by the final state repulsion of the two electrons and selection rules resulting from the $^1P^0$ symmetry of the final two-electron state [1]. One might expect that the final state repulsion is similar for H_2 and He since the photoelectrons are much faster than the heavy nuclei. Hence, at large distances, the electrons

move in the Coulomb field of a point charge $Z = 2$. Thus a heliumlike model [9,10] described well the measurements [5] from randomly oriented D_2 molecules. Feagin [9] introduced two complex symmetrized amplitudes, g_Σ and g_Π, for the PDI by light polarized along and perpendicular to the molecular axis, respectively.

Despite this similarity of the PDI of He and H_2 some selection rules that exclude certain escape geometries are relaxed for H_2 ([9,11]). Primarily, this relaxation stems from the loss of a fixed angular momentum for the photoelectron pair; i.e., the electronic continuum wave function does not have pure P symmetry. The molecular ground state contains high angular momentum components and electron scattering by the nuclei during escape can mix angular momenta.

In helium, for equal energy electrons, the cross section is zero on a cone $\theta_2 = 180° - \theta_1$, where $\theta_{1,2}$ are the polar angles of electrons 1 and 2 with respect to the polarization axis (see selection rule F in Fig. 1 and [1]). In the case of the coplanar geometry (light polarization axis in the plane of the electron momenta) this rule forbids back-to-back emission. Parity conservation also forbids equal energy back-to-back emission (selection rule C in Fig. 1 and [1]); thus for He this configuration is doubly forbidden. For H_2, only the back-to-back emission is forbidden [11]; the rest of the cone is accessible for most molecular orientations. Until recently, this prediction was confirmed only indirectly by coplanar measurements from randomly oriented molecules. Our new measurements show that the change of symmetry and the related relaxation of the $\theta_2 \neq 180° - \theta_1$ selection rule are clearly visible for out-of-plane geometries. We find that the atomiclike description of the PDI of H_2 due to Feagin [9] remains a good approximation, and we reproduced qualitatively our
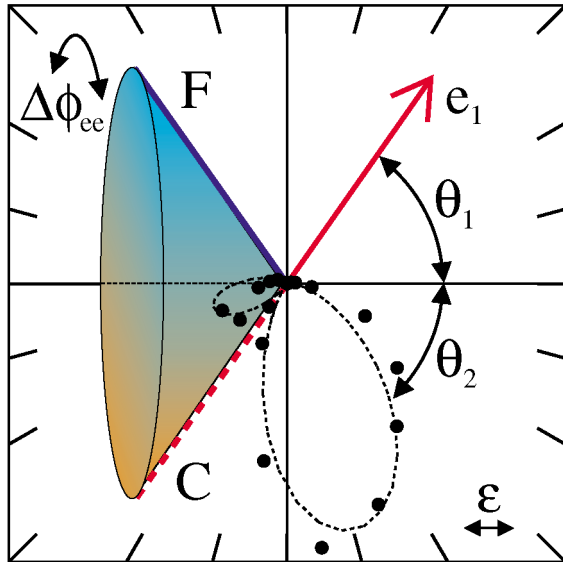
FIG. 1 (color online). Illustration of the selection rules: The dots show the FDCS for the PDI of helium at 24 eV above threshold for equal energy sharing $[E_1/(E_1 + E_2) = 0.5 \pm 0.1]$. The polarization axis is horizontal. The first electron is fixed at $\theta_1 = 55° \pm 12°$ (arrow). For equal energies, the two-electron states with $^1P^0$ symmetry (final state in the PDI of He) have a node for $\theta_2 = 180° - \theta_1$ indicated by the cone (selection rule F), where $\theta_{1,2}$ are the polar angles of electrons 1 and 2 with respect to the polarization axis (see [12]). The dashed straight line indicates the forbidden back-to-back emission (selection rule C). The dashed curve is a fit to the data using the Gaussian parameter $\theta_{12} = 99.5° \pm 1.5°$ (see, e.g., [9] and references therein).

measurements by calculating g_Σ and g_Π using a single-center model.

The COLd Target Recoil Ion Momentum Spectroscopy (COLTRIMS) technique [13] was used to measure the momenta of all the particles in fourfold coincidence. The 2-bunch mode photon beam at beam line 7.013 of the Advanced Light Source at LBNL intersected a supersonic molecular beam of D_2 (D_2 has higher target density than a comparable H_2 jet and yields data with fewer random coincidences from background H_2O). The particles were guided by electric and magnetic fields onto two position sensitive channel plate detectors that registered multiple hits on rectangular and hexagonal delay-line anodes (see [14]). We did two experiments (~8 days each) at the same photon energy using different guiding field and spectrometer configurations. In both, the fields assured 4π collection efficiency for all particles. However, a multihit dead time on the electron detector and a vanishing momentum resolution for electrons performing integer revolutions in the solenoid magnetic field (see [15]) yielded some dead areas in the multidimensional phase space of each experiment. The geometry and fields were chosen so that the observed regions of phase space were complimentary. One experiment used a weak elec-

tric field for the electron collection followed by a high pulsed field for the ion collection. Each experiment included measurements on He at the same excess energy using the same spectrometer settings. Since He results are well established, these gave independent checks of the experimental setups.

The FDCS $d\sigma^7/d\theta_1 d\theta_2 d\Delta\phi_{ee} d\theta_R d\Delta\phi_{eR} dE_1 dE_2$ depends on the polar angles $\theta_{1,2,R}$ of electrons 1 and 2 and the internuclear axis R with respect to the polarization axis, on the difference of the azimuthal angles $\Delta\phi_{ee} = \phi_1 - \phi_2$ of the two electrons, the difference between the azimuthal angles of the first electron and the molecular axis $\Delta\phi_{eR} = \phi_1 - \phi_R$, and on the electron energies E_1, E_2. Figure 2 shows the FDCS for D_2 at different molecular orientations, and, for comparison, results for helium. The helium results [Fig. 2(d)] display the well-known structure of two lobes separated by the area at $\theta_2 = 180° - \theta_1$ (forbidden by selection rule F). This is indicated by the vertical dashed line equivalent to the cone shown in Fig. 1 (see also Fig. 11 in Ref. [16] and Fig. 2 in Ref. [12]). As predicted by Walter and Briggs (selection rules H and I in [11]), the nodal cone, and hence the He-like FDCS, is also observed for D_2 with its molecular axis parallel or perpendicular to the polarization of light where only one amplitude f_Σ (not shown here) or f_Π [Fig. 2(c)] contributes to the PDI. For arbitrary orientation of the molecule, the cone fills up due to interference of the f_Σ and f_Π amplitudes; this is weighted by the factor $\cos\theta_R \cdot \sin\theta_R$ and hence is strongest at $\theta_R = 45°$. Indeed, for D_2 at $\theta_R = 45°$ the forbidden area is reduced to a singular node for back-to-back emission [dot in Fig. 2(a): selection rule C]. After integration over all molecular orientations [Fig. 2(b)] the filling of the node is less prominent because of the dominating Π transition (compare with [2]). Note that the maximum for D_2 (vs that for He) is slightly shifted to the left. This is consistent with observations in the coplanar geometry ([4–7]), which corresponds to a slice through Fig. 2(b) along the $\Delta\phi_{ee} = 0°$ and $\Delta\phi_{ee} = 180°$ line. The authors of Refs. [4–7] also observed a slight filling of the node for back-to-back emission; this was ascribed to a finite experimental acceptance angle in $\Delta\phi_{ee}$ ([9,10]) and is present in our measurements as well.

The coplanar geometry where the electron momenta, molecular, and polarization axes are in the same plane ($\Delta\phi_{ee} = 0°, 180°$ and $\Delta\phi_{eR} = 0180°$) displays in more detail the influence of the molecular axis orientation on the photoelectron angular distributions as shown Fig. 3 for equal energy sharing. The measurements in 3(a) are integrated over all molecular orientations. The solid line [in 3(a)] shows the spherically averaged FDCS calculated using Eq. (6) of Feagin [9]. To evaluate the amplitudes f_Σ and f_Π, we used a single-center expansion model of the H_2 ground state [17], and a convergent close-coupling expansion of the final two-electron state in the field of a pointlike charge $Z = 2$ [18]. For comparison, the
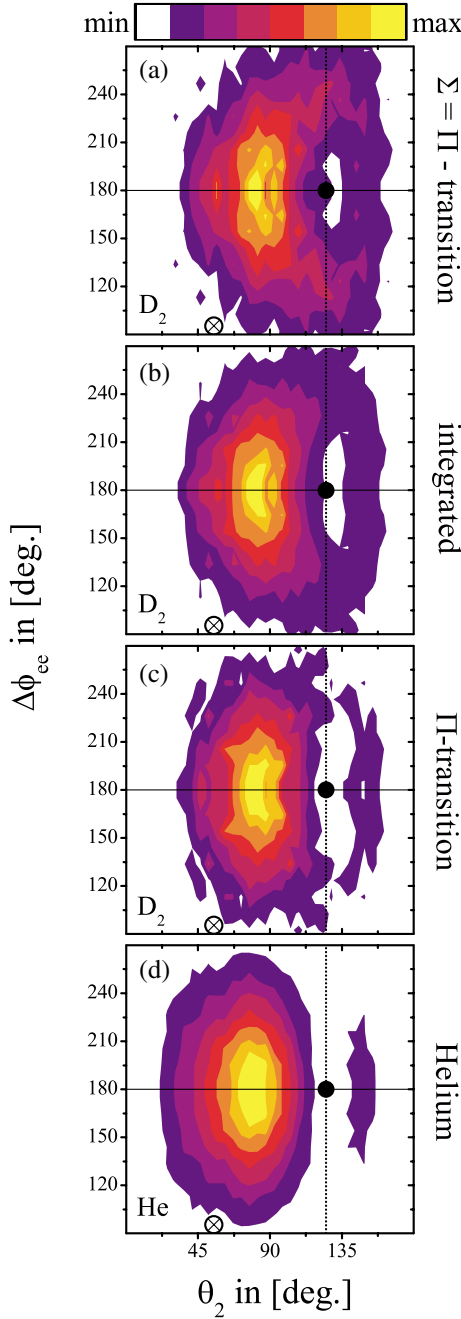
FIG. 2 (color online). A density plot of the angular distribution of the second electron when the first electron is detected at $\theta_1 = 55° \pm 12°$ (circled cross). The patterns show the PDI of D_2 (a)–(c) at 75.5 eV and He (d) at 103 eV photon energy (sum electron energy 24 eV), equal energies $[E_1/(E_1 + E_2) = 0.5 \pm 0.1]$, and linearly polarized light. Horizontal axis: polar angle θ_2 of electron 2 with respect to the polarization axis, vertical axis: difference between the azimuthal angles of the two electrons $\Delta\phi_{ee}$. The back-to-back emission is at the full dot on the $\Delta\phi_{ee} = 180°$ line. The dashed vertical line is the nodal cone $\theta_2 = 180° - \theta_1 = 125°$. The color scale is linear in the count rate. (a) D_2 molecule $\theta_R = 45° \pm 11°$, i.e., a mixture of Σ and Π transition (integrated over $\Delta\phi_{eR}$); (b) D_2 integrated over all molecular orientations; (c) $\theta_R = 90° \pm 11°$, i.e. Π transition (integrated over $\Delta\phi_{eR}$); (d) results from helium.
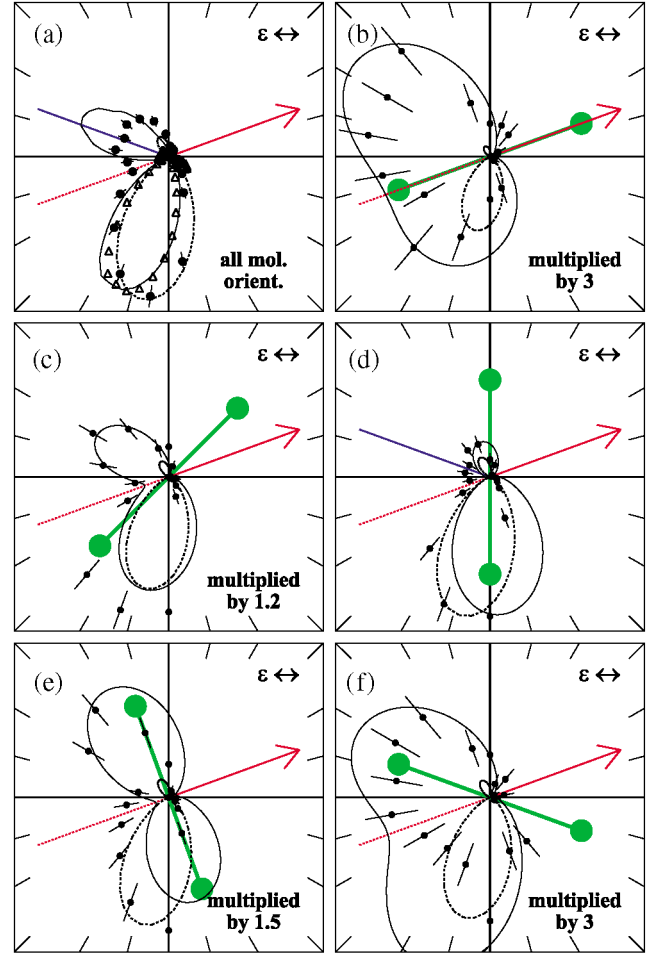

FIG. 3 (color online). FDCS for PDI of D_2, for equal energies $E_1/(E_1 + E_2) = 0.5 \pm 0.1$, $\theta_1 = 20° \pm 10°$ (arrows), polarization horizontal, and electron 2 coplanar. (a) Integrated over all molecular orientations. (b)–(f) molecule coplanar ($\Delta\phi_{eR} = 0°, 180° \pm 45°$) and (b) $\theta_R = 20°$, (c) $\theta_R = 45°$, (d) $\theta_R = 90°$, (e) $\theta_R = 110°$, (f) $\theta_R = 160°$ (all $\pm 12°$). The data are internormalized for all angles θ_R; the multiplier used is indicated in each panel. The calculation (solid lines) corresponds to Eqs. (5) and (6) of Feagin [9] on (a) and (b)–(f), respectively. The open triangles in (a) show the same calculation with $f_\Sigma = f_\Pi$. The dashed lines show the Gaussian fit to the helium calibration data of this measurement (similar to Fig. 1). The dashed line indicates selection rule C. The solid line in (a) represents selection rule F valid on a cone in the PDI of helium.

interference-free FDCS calculated with $f_\Sigma = f_\Pi$ (open triangles) is shown. The interference of f_Σ and f_Π causes the main lobe in the spherically averaged FDCS for D_2 which is slightly shifted backwards, i.e., here the two electrons repel each other more strongly than in the case of helium. This is also seen in the measurements. The more prominent difference revealed by the measurements, however, is the increase of the upper lobe; this is also seen in the single-center calculation (solid line). The filling of the node for back-to-back emission is due to the large acceptance angle in $\phi_{ee} = 180° \pm 30°$ [4,5,10].

The difference between D_2 and He, while not striking in the averaged data [Fig. 3(a)], is marked when appropriate conditions are chosen. For example, there are strong changes in the electron angular distribution as the molecular orientation is varied with respect to the light polarization [Figs. 3(b)–3(f)]. Only for a pure Σ (not shown here) and Π transition [3(d)] is a structure similar to He observed. At other orientations, the upper lobe, negligible for He, is much stronger or dominates for D_2. This dramatic change in the angular distributions reflects the impact of the interplay of selection rules and electron repulsion on the FDCS. The $\theta_2 \neq 180° - \theta_1$ selection rule (cone in Fig. 1) holds exactly for He and for the pure Σ or Π transition in D_2 and leads to nodes along the dashed and solid lines in Fig. 3(d) (Π transition). However, for molecular orientations other than 0° and 90°, only the singular nodal point of the back-to-back emission [selection rule C, dashed line] survives; the node in the upper half plane vanishes. Hence the significant electron flux observed in the upper half plane is a direct consequence of the interference of the g_Π and g_Σ amplitudes.

The solid lines on panels 3(b)–3(f) show the calculated FDCS obtained from the single-center amplitudes in Eq. (5) of [9]. The calculation is convoluted with the finite spreads in the acceptance angles and energy sharing ratio. The results reproduce the main features of the experiment. Not only the shape but also the cross section changes strongly with the molecular axis rotation (see scaling factors and Fig. 3 caption). It is noteworthy that a Gaussian parametrization applies well to both amplitudes g_Π and g_Σ giving their magnitude ratio $g_\Pi/g_\Sigma = -1.1$ and their FWHM $\Delta\theta_{12}^\Sigma = 70.0°$ and $\Delta\theta_{12}^\Pi = 78.8°$ (compare also to [9]). Fitting our experimental data yields $\Delta\theta_{12}^\Sigma = 83.5°$ and $\Delta\theta_{12}^\Pi = 61.5°$.

In summary, we have observed significant differences in the FDCS of He and D_2 for the noncoplanar geometry and for mixed Σ and Π transitions. The coplanar geometry is well reproduced by the He-like theory [9] with a pair of amplitudes g_Σ and g_Π. Interference of these yields the strong dependence of the FDCS on the molecular orientation. We calculated the amplitudes using the single-center expansions for the molecular ground state and the final two-electron state. The similarity between the theoretical and experimental FDCS indicates that much of the angular correlation pattern is formed by the electron-electron correlation in the final state at fairly large distances from the molecular ion. The nonzero angular momentum components of the molecular ground state also play a role. In spite of the success of the single-center He-like model, a full molecular calculation remains desirable for comparison with these and future results.

*Electronic address: doerner@hsb.uni-frankfurt.de
[1] J. Briggs and V. Schmidt, J. Phys. B **33**, R1 (2000).
[2] H. Kossmann, O. Schwarzkopf, B. Kämmerling, and V. Schmidt, Phys. Rev. Lett. **63**, 2040 (1989).
[3] G. Dujardin, Phys. Rev. A **35**, 5012 (1987).
[4] T. J. Reddish, J. P. Wightman, M. A. MacDonald, and S. Cvejanovic, Phys. Rev. Lett. **79**, 2438 (1997).
[5] J. Wightman, S. Cvejanovic, and T. J. Reddish, J. Phys. B **31**, 1753 (1998).
[6] S. A. Collins, A. Huetz, T. J. Reddish, D. P. Seccombe, and K. Soejima, Phys. Rev. A **64**, 062706 (2001).
[7] D. P. Seccombe, S. A. Collins, T. J. Reddish, P. Selles, L. Malegat, A. K. Kazansky, and A. Huetz, J. Phys. B **35**, 3767 (2002).
[8] R. Dörner *et al.*, Phys. Rev. Lett. **81**, 5776 (1998).
[9] J. M. Feagin, J. Phys. B **31**, L729 (1998).
[10] T. J. Reddish and J. M. Feagin, J. Phys. B **32**, 2473 (1999).
[11] M. Walter and J. S. Briggs, Phys. Rev. Lett. **85**, 1630 (2000).
[12] F. Maulbetsch and J. Briggs, J. Phys. B **28**, 551 (1995).
[13] R. Dörner, V. Mergel, O. Jagutzki, L. Spielberger, J. Ullrich, R. Moshammer, and H. Schmidt-Böcking, Phys. Rep. **330**, 95 (2000).
[14] O. Jagutzki *et al.*, IEEE Trans. Nucl. Sci. **49**, 2477 (2002).
[15] R. Moshammer *et al.*, Nucl. Instrum. Methods Phys. Res., Sect. B **107**, 62 (1996).
[16] R. Dörner, V. Mergel, L. Spielberger, O. Jagutzki, J. Ullrich, and H. Schmidt-Böcking, Phys. Rev. A **57**, 1074 (1998).
[17] H. W. Joy and R. G. Parr, J. Chem. Phys. **28**, 448 (1958).
[18] A. S. Kheifets and I. Bray, J. Phys. B **31**, L447 (1998).